International Journal of Heat and Mass Transfer 138 (2019) 11–16

Contents lists available at ScienceDirect

International Journal of Heat and Mass Transfer

journal homepage: www.elsevier.com/locate/ijhmt

A general method for measuring the thermal conductivity of MOF crystals

Jun Huang [a], Xiaoxiao Xia [b,c], Xuejiao Hu [a,*], Song Li [b,c,*], Kang Liu [a,*]

[a] MOE Key Laboratory of Hydraulic Machinery Transients, School of Power and Mechanical Engineering, Wuhan University, Wuhan 430072, Hubei, China
[b] State Key Laboratory of Coal Combustion, School of Energy and Power Engineering, Huazhong University of Science and Technology, Wuhan 430074, Hubei, China
[c] China-EU Institute for Clean and Renewable Energy at Huazhong University of Science and Technology, Wuhan 430074, Hubei, China

ARTICLE INFO

Article history:
Received 28 November 2018
Received in revised form 19 February 2019
Accepted 4 April 2019

Keywords:
Metal-organic framework
Thermal conductivity
Water adsorption
Effective media approximation

ABSTRACT

Thermal conductivity is a critical parameter for metal-organic framework (MOF) in many practical applications. However, experimental measurement of the thermal conductivity of MOF crystals is of great challenge due to its small size. Herein, we proposed a general method to obtain the thermal conductivity of MOF crystal using MOF powder sample. By measuring the thermal conductivity of compacted MOF powders at varying water contents using transient hot-wire method, the thermal conductivity of MOF crystal can be derived by a biporous effective medium approximation (BEMA) model. The eventually obtained thermal conductivities of three different MOF crystals: UiO-66, UiO-67 and Cu-BTC, are 0.11 W/(m·K), 0.19 W/(m·K), and 0.39 W/(m·K), respectively, consistent with previously reported results of MOF crystals.

1. Introduction

Metal-organic frameworks (MOFs) have attracted increasing attention due to their unique structure properties [1,2] in a variety of applications, including gas storage [3,4], chemical separation [5], catalysis [6], sensing [7], and water harvesting from air [8,9]. MOF adsorbents will release/absorb heat during gas adsorption/desorption processes. Such exothermic or endothermic process will significantly change the temperature of MOF adsorbents, and sequentially affect the mass transfer and gas storage capacity [10]. Low thermal conductivity of MOFs may also slow down the refuelling of hydrogen storage tank [11]. Therefore, thermal management of MOFs is crucial for rapid and efficient gas adsorption, and thermal conductivity of MOF crystal may provide crucial insights into the thermal manipulation of MOF-based gas storage systems. However, experimental measurement of the thermal conductivity of MOF crystals is very challenging because of the small size of MOF crystals.

A vast majority of experimental measurements of the MOF thermal conductivity were implemented on compacted MOF powders, which usually exhibited lower thermal conductivities (below 0.1 W/(m·K) [12–16]) than pristine MOF crystals. It is because the large thermal contact resistance between MOF particles. Moreover, the contribution of contact resistances to the total thermal conductivity is very difficult to be quantified for the compacted powder sample. Thus, it is a great challenge to derive the thermal conductivity of pristine MOF crystals from the measured effective thermal conductivity of compacted MOF powders. This is a common issue not only for the compacted powder of MOFs but also for carbon nanotubes, graphene sheets and other nanoparticles [17]. Direct measurement of the thermal conductivity of MOF crystal can be a challenge due to the requirement of large-size single crystal in millimeters. Until now, only a very few types of MOF crystals that can grow to a suitable crystal size have been measured by 3ω technique or steady-state measurements. The obtained thermal conductivities from single-crystal ZIF-8 [18], MOF-1 [19], and MOF-5 [20], at room temperature are 0.33 W/(m·K), 1.3 W/(m·K) and 0.32 W/(m·K), respectively, which agrees with the predicted results from molecular dynamics (MD) simulations (0.31 W/(m·K) for MOF-5 [21] and 0.165 W/(m·K) for ZIF-8 [22]). Given the difficulty in preparing large-size single crystals for a large number of MOFs, there is a great need to develop a novel technique to acquire the thermal conductivity of small-size MOF crystals using the sample of compacted MOF powders.

* Corresponding authors at: MOE Key Laboratory of Hydraulic Machinery Transients, School of Power and Mechanical Engineering, Wuhan University, Wuhan 430072, Hubei, China (K. Liu, X.J. Hu); State Key Laboratory of Coal Combustion, School of Energy and Power Engineering, Huazhong University of Science and Technology, Wuhan 430074, Hubei, China (S. Li).

E-mail addresses: xjhu@whu.edu.cn (X. Hu), songli@hust.edu.cn (S. Li), kang.liu@whu.edu.cn (K. Liu).

https://doi.org/10.1016/j.ijheatmasstransfer.2019.04.018
0017-9310/

Herein, we proposed a general method to obtain the thermal conductivity of small-size MOF crystal by measuring the compacted MOF powder under varying water contents. The compacted MOF powder is taken as a hierarchical system consisting of pristine MOF crystals, macropores formed by MOF particles in contact, and micropores inside MOF crystals. Micropores inside MOFs are preferentially occupied by adsorbed water molecules under humid conditions, followed by macropores formed by MOF crystal particles. Hence, at low water contents, the adsorbed water molecules will increase the thermal conductivity of MOF crystals rather than inter-particles thermal contact conductance. Assuming the constant inter-particle thermal contact resistance between MOF crystals at low water contents, the thermal conductivity of MOF crystal and the inter-particle contact resistance can be derived separately based on our Biporous Effective Medium Approximation (BEMA). The strategy proposed in this study may open up a possibility to obtain the thermal conductivity of a tiny MOF crystal by a simple and general method.

2. Experimental procedures

2.1. Materials preparation and characterization

All chemicals in this study were used as received (without any purification) from commercial sources. UiO-66 [23], UiO-67 [24] and Cu-BTC [25] were prepared according to the previous reports with slight modifications. The crystallinity of MOFs structures was confirmed by powder X-ray diffraction (PXRD) patterns (Empyrean, PANalytical, Netherlands). Nitrogen adsorption isotherms measured at 77 K by gas adsorption analyzer (Autosorb-iQ2, Quantachrome Instruments, USA) were used to derive the BET surface area, and the total pore volume. The pore size of MOFs was determined by NLDFT model according to nitrogen adsorption isotherms.

In order to derive the thermal conductivity of MOF crystals, both the true densities and sizes of pristine MOF crystals (particles) are required parameters. The densities of MOF crystals were directly measured by True Density Analyzer (AccuPyc 1330, Micromeritics Instrument, USA). The sizes of MOF crystals were statistically calculated based on 10 images of scanning electron microscopy (SEM) (Quanta 200, FEI NanoPorts, Netherlands) for each type of MOFs. Eventually, the particle size distribution of each MOF was obtained as shown in Fig. S1.

2.2. Thermal conductivity measurement

The thermal conductivities of compacted MOF powders were measured with a classical transient hot-wire method as demonstrated in Fig. S2. In details, MOF powders were placed in a box of 20 mm × 5 mm × 6 mm located in the center of two polymethyl methacrylate (PMMA) plates. A platinum wire with a diameter of 18.5 μm was placed in the center of MOF powders as a heater and temperature sensor. The effective thermal conductivity of compacted MOF powder sample was derived by probing the temperature rise of the platinum wire upon being heated under constant power. The heat conduction process in this system can be taken as a one-dimensional problem in cylindrical coordinate system, with the governing equation:

$$\frac{1}{\alpha}\frac{\partial T}{\partial t}=\frac{\partial^2 T}{\partial t^2}+\frac{1}{r}\frac{\partial T}{\partial r} \tag{1}$$

In this case, semi-infinite boundary condition with constant heat flux at the interface between platinum wire and MOF powders was employed. The region is initially at constant temperature. Solving Eq. (1) yields

$$T=\frac{q}{4\pi k}\left[\ln(t)+\ln\left(\frac{4\alpha}{r_0^2}\right)-\gamma\right] \tag{2}$$

T is the increased temperature of the hot wire; q is the constant heat flow applied along the platinum wire; k and α are the effective thermal conductivity and diffusivity of the MOF powders, respectively; r_0 is the radius of the platinum wire; γ represents the Euler constant; t is the time. From Eq. (2) we can obtain the thermal conductivity k with $k = q/(4\pi \cdot b)$. b is the slope obtained by fitting the curve of temperature rise with the logarithm of heating time as shown in Fig. S3. The system error of our hot-wire measurement was estimated to be 3.7% according a calibration experiment using polydimethylsiloxane (PDMS).

The temperature of the platinum wire can be derived from the resistance of the wire, which was obtained from the operating current and voltage recorded by a commercial data acquisition system (NI 9205 data acquisition card and cDAQ-9174 chassis). Different amounts of water uptakes were achieved by tuning the exposure time to saturated water vapor. The increased water contents of compacted MOF powder were calculated from the variation in the system mass. The duration of each test was within 50 ms to minimize water desorption due to Joule heating of the platinum wire and ensure the semi-infinite boundary condition for thermal conduction.

3. Results and discussion

Here we tested three kinds of MOFs: UiO-66, UiO-67 and Cu-BTC. Fig. 1 shows the morphology, SEM images and PXRD patterns of UiO-66, UiO-67 and Cu-BTC, respectively. According to the SEM images, the MOF crystals have characteristic sizes of micrometers, which is several orders of magnitude smaller than that of MOF-5 [20] and ZIF-8 [18]. The measured PXRD patterns in the insets of Fig. 1d–f are consistent with the simulated results, indicating that the prepared samples have high purity and crystallinity. BET surface area, pore size, pore volume and true density of MOFs are summarized in Table 1.

In order to derive the thermal conductivity of MOF crystals, we measured the effective thermal conductivity of compacted MOF powders under varying water contents. The experiment setup is as shown in Fig. S2, which is a classical transient hot-wire setup. With the increase of water contents, the thermal conductivity of compacted MOF powder may be remarkably increased given the high thermal conductivity of water (0.6 W/(m·K)). However, although the thermal conductivity of compacted UiO-66 (0.023 W/(m·K)), UiO-67 (0.024 W/(m·K)) and Cu-BTC (0.04 W/(m·K)) powders increased with water contents, the enhancement was not as significant as expected (shown as Fig. 2). As we know, compacted MOF powder is a hierarchical porous system consisting of macropores (interspace) formed by MOF particles in contact and micropores exiting inside MOFs. Water molecules are preferentially adsorbed in micropores inside MOFs [26,27] instead of the interspace between MOF particles. Thus we assume that, at low water contents, the adsorbed water directly promotes the thermal conductivity of MOF particles themselves, while the inter-particle contact resistances will not change during adsorption. Such assumption explained why the effective thermal conductivities of MOF powders do not increase remarkably with water contents, given the high inter-particle contact resistance in powder systems of micro- or nano-particles [17].

To further support our assumption, we increased the water content of Cu-BTC powder gradually to 98%. At high water contents, micropores inside MOF crystals were saturated. Surplus water started to occupy the interspace between MOF particles, which would significantly reduce the inter-particle contact resistances [28]. Hence the effective thermal conductivity of MOF powder

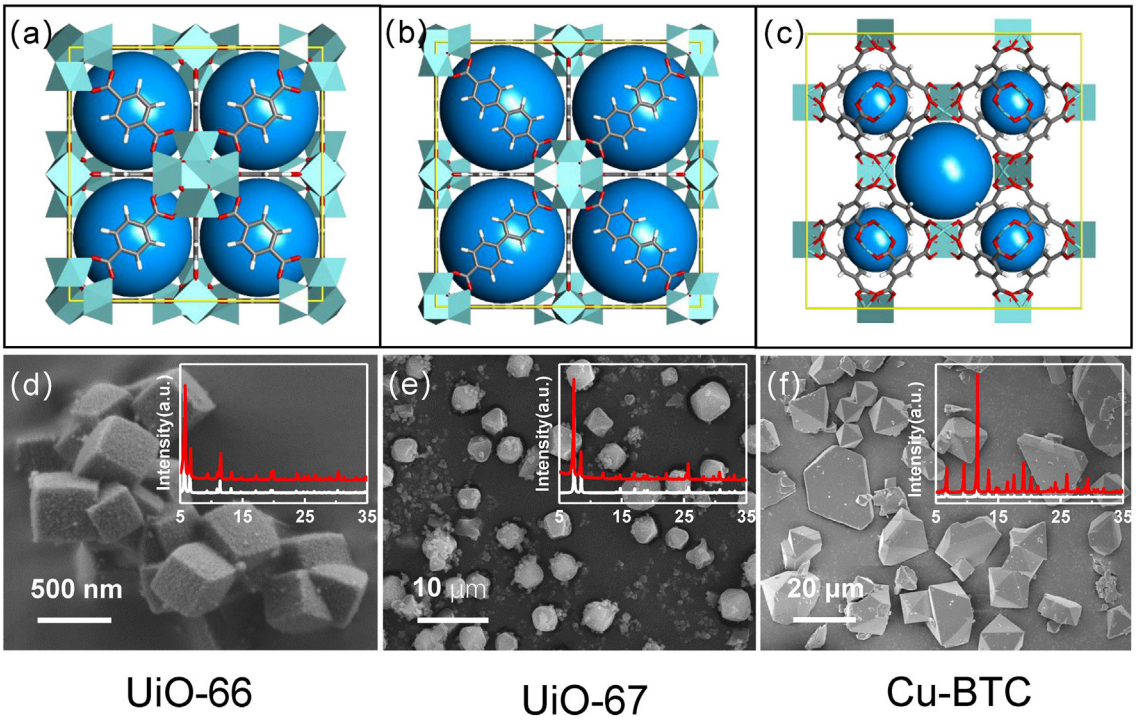

Fig. 1. Crystal structure, SEM images and PXRD results of UiO-66, UiO-67, and Cu-BTC, respectively. (a)–(c) are atomic structures. (d)–(f) are the corresponding SEM images. Inserts are the XRD results. Red lines are experiment results and white lines are simulation results. (For interpretation of the references to colour in this figure legend, the reader is referred to the web version of this article.)

Table 1
Structural parameters of the MOFs.

Samples	BET measurement (m^2/g)	Void volume[a] (cm^3/g)	True density[b] (g/cm^3)	Particle density[c] (g/cm^3)	Pore radius (nm)	Effective radius of crystal particle[d] (μm)
UiO-66	1386	0.672	1.703	0.794	0. 531	0.12
UiO-67	2471	1.013	1.742	0.630	0.716	1.57
Cu-BTC	1830	0.8414	1.66	0.693	0.224	6.20

[a] The void volume determines maximum amount of water uptake.
[b] True density was tested by AccuPyc 1330, Micromeritics Instrument, USA, representing the MOF crystal density (except micro pores inside MOF particle).
[c] MOF particle density was calculated from the true density and the void volume to determine the porosity of the tested powder sample.
[d] The effective radius of crystal particle was obtained by counting the particle size from SEM topographies, which was used to quantity the contact numbers of MOF powder samples.

increased rapidly with water content as shown in high-water-content region (>26%) of Fig. 2d. For comparison, the increasing rate at low-water-content region is much slower, which indicates a mechanism of thermal conductivity promotion not relevant to contact resistances. These results indirectly support our assumption that, small amount of water uptakes in MOF powders only tune the thermal conductivity of MOF particles and will not change the inter-particle contact resistances. Based on such assumption, the thermal conductivity of MOF crystals (k_{cryst}) and inter-particle resistance in MOF powders can be separately derived from the dependence of effective conductivity of MOF powders on water contents.

In order to derive the thermal conductivity of MOF crystal (k_{cryst}) from the measured thermal conductivity (k_{eff}) of compacted powders, we proposed a Biporous Effective Medium Approximation (BEMA) model, in which the MOFs particles are distributed as shown in Fig. 3a. Each MOF particle is assumed to be a multi-phase composite consisting of pristine MOF crystal (continuous phase), adsorbed water and air in the micropores of MOFs (discontinuous phases). The thermal conductivity of a MOF particle (k_p) consisting of MOF crystal, adsorbed water and air can be calculated by a three-component Maxwell-Garnett Effective Medium Approximation [29,30] shown below

$$k_p = \frac{k_{cryst} v_{cryst} + k_{air} v_{air} f_{air} + k_{H_2O} v_{H_2O} f_{H_2O}}{v_{cryst} + v_{air} f_{air} + v_{H_2O} f_{H_2O}} \quad (3)$$

k_{cryst}, k_{H_2O} and k_{air} are thermal conductivities of MOF crystal, adsorbed water and air in the pores, respectively. v_{cryst}, v_{H_2O} and v_{air} represent the volume fractions of MOF crystal, adsorbed water and air, respectively. f_{H_2O} and f_{air} are defined as $3k_{cryst}/(2k_{cryst} + k_{H_2O})$ and $3k_{cryst}/(2k_{cryst} + k_{air})$, respectively. The thermal conductivity of air in the pore can be calculated as $k_{air} = 2r_0\, k_{air0}/\Lambda$, in which r_0 is the radius of pores inside MOF crystal, and Λ is the mean free path of air, and k_{air0} is the thermal conductivity of free air. Eq. (3) was derived by assuming that there is no interfacial resistance for MOF crystal/adsorbed water and MOF crystal/air interfaces.

In order to establish the relationship between thermal conductivity of MOF particles and the effective thermal conductivity of compacted MOF powders, we then employed a simplified model to describe the structure of MOF powders. Four assumptions were made: (i) thermal convection and radiation are negligible; (ii) interfacial thermal resistance between the solid phase and gas/liquid phase is negligible; (iii) MOF crystal particles are spherical shaped; (iv) MOF crystal particles tangent to each other are uniformly dispersed in a finite region. Thus, the powder system can be sliced into multiple layers with the width of d along the direc-

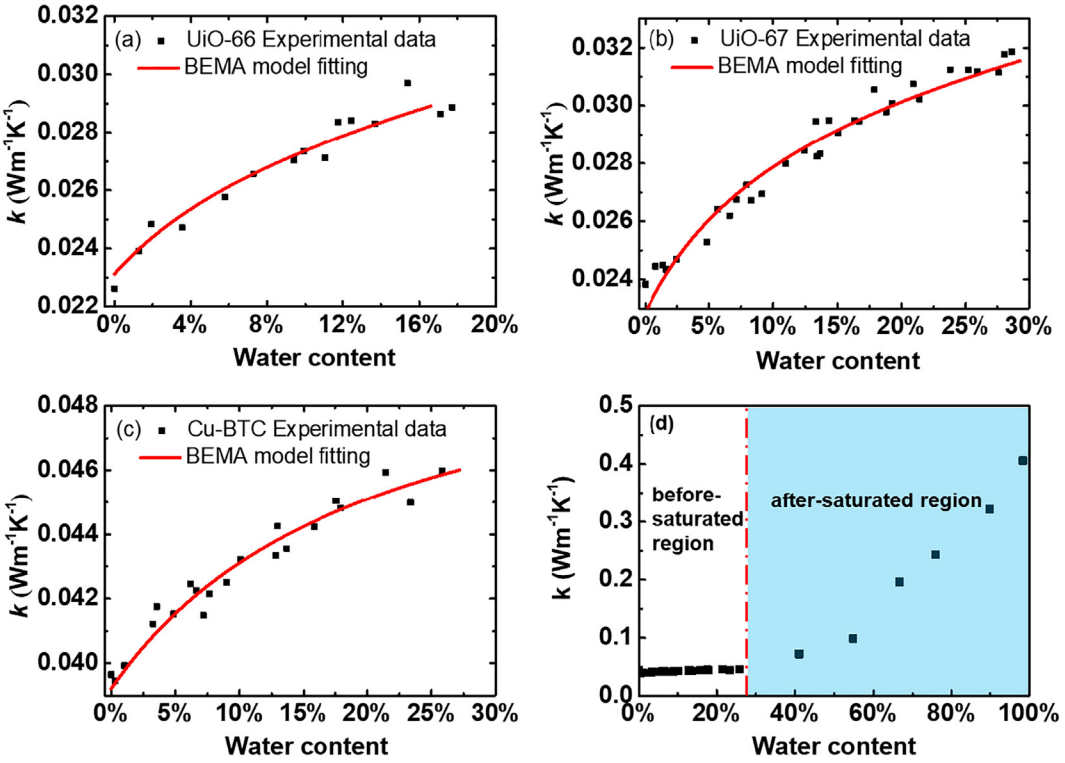

Fig. 2. Dependence of the packed beds' thermal conductivity on the amount of adsorbed water. (a, b, c) Experimental results and theoretical fitting of UiO-67 (a), UiO-66 (b) and Cu-BTC (c) packed beds, respectively. Black squares are the experimental data and red lines are the fitting curves with the BEMA model. (d) Thermal conductivity variation of Cu-BTC packed bed with different amount of adsorbed water in before- and after- saturated region.

tion of heat flow, where d is the diameter of a MOF particle. Each layer was filled with complete spheres in contact as shown in Fig. 3b, similar to previous studies [31,32]. The number of particles in each layer per unit area is $M = 3(1-\phi)/(2\pi r^2)$, in which ϕ is the porosity of the MOF powder sample that can be calculated according to the measured true density of MOFs, and r is the radius of a MOF particle. The effective number of contacts (n) of one MOF particle can be empirically calculated as [33] $n = 13.84–(232(1–\phi)–57.8)^{0.5}$. To obtain the thermal conductivity of one layer, we divided a single layer into multiple heat transfer unit cells as shown in the top right of Fig. 3b. Herein, each cylindrical unit cell consists of one solid sphere and the void interspace around. Effective thermal conductivity of the unit cell (k_{unit}) can be written as [34,35]:

$$k_{unit} = \frac{2k_{air0}}{1-\beta}\left(\frac{1}{1-\beta}\ln\frac{1}{\beta} - 1\right) \quad (4)$$

where $\beta = k_{air0}/k_p$. The inter-particle contact resistances (the reverse of contact conductance) can be treated as resistance in-series with the effective thermal resistance of the unit cell. Thus, the total thermal resistance of each layer is equal to the thermal resistance of unit cells (including contact resistance) and the thermal resistance of air gap in this layer are in parallel as shown in Fig. 3c. Eventually, the measured effective thermal conductivity (k_{eff}) can be computed using Eq. (5) shown below.

$$k_{eff} = \frac{2r}{1/(2/(M\cdot\pi\cdot r\cdot k_{unit}) + 2/(G\cdot n\cdot M) + 1/R_g)} \quad (5)$$

where G is the contact conductance between MOF particles, and R_g is the thermal resistance of air gap that can be computed by $R_g = 2r/(k_{air}\cdot(1-n\pi r^2))$.

According to Eqs. (3)–(5), the effective thermal conductivity of compacted MOF powders (k_{eff}) can be theoretically calculated from k_{cryst} and G. Thus, we can derive k_{cryst} and G by fitting Eq. (5) to the experimental results of k_{eff}. Here an important point should be noted is that k_{cryst} and G imposed different impacts on the dependence of k_{eff} on the water content (see Fig. S5). k_{cryst} mainly affects the theoretical curve at low water contents and does not change the curve too much at high water contents, because the thermal conductance of MOF crystal is much smaller than that of adsorbed water at high water contents. G mainly affects the fitting curve at high water contents, because G becomes the determinative thermal resistance of the system when thermal conductance of MOF particles is high enough at high water contents. Herein, the different impacts of k_{cryst} and G on the fitting curve are important prerequisites for deriving k_{cryst} and G, separately.

Eventually, the derived thermal conductivities of MOF crystals and inter-particle contact conductance were presented in Table 2. The thermal conductivity of UiO-66, UiO-67 and Cu-BTC are 0.11 W/(m·K), 0.19 W/(m·K), and 0.39 W/(m·K), respectively, which are in the same order of magnitude with previously reported thermal conductivity of MOF crystals from simulations or experiments (i.e. 0.32 W/(m·K) of MOF-5 [20], 0.326 W/(m·K) of ZIF-8 [18]). Among three MOFs, Cu-BTC crystal exhibited the highest thermal conductivity. UiO-67 and UiO-66 possess the same central atoms and organic chains, but UiO-67 showed higher thermal conductivity than UiO-66. The thermal conductivity of MOF crystal increases with the pore size, which is probably due to the fewer resistive junctions per unit length for UiO-67 as suggested by Han et al. [36]. The inter-particle contact conductance of UiO-66, UiO-67 and Cu-BTC are 0.0117 μW/K, 0.09 μW/K and 0.82 μW/K, respectively, which are reversely correlated with the porosity of MOF powder samples.

Considering the error of transient hot wire measurements and numerical fitting (shown in Fig. S3, S5), the uncertainty of our measurements is 30% for thermal conductivity of MOF crystal and 10% for the contact resistance. Here the uncertainty comes from two

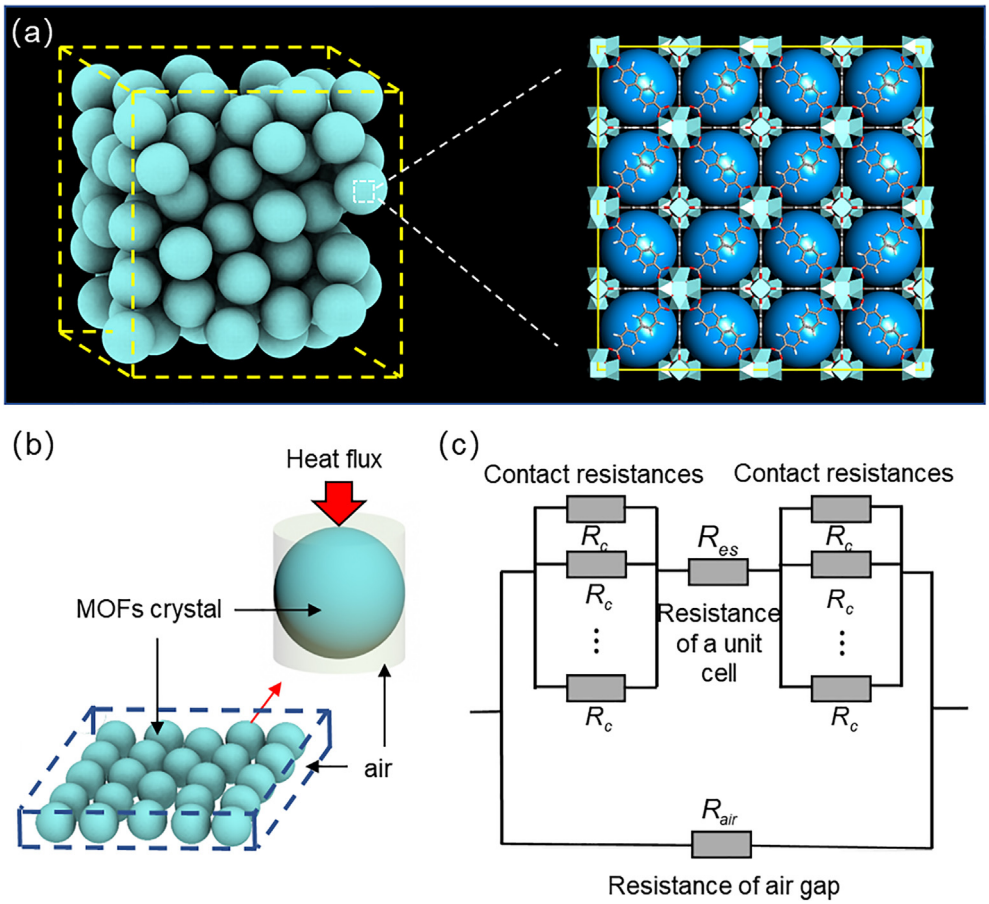

Fig. 3. Schematic of the two-level effective media approximation model for a MOF packed bed. (a) Schematic of the structure of the MOF packed beds. The porosities of MOF particles are 0.73, 0.54, 0.53 for UiO-66, UiO-67, and Cu-BTC packed bed, respectively. (b) Schematic of a unit heat transfer layer in the MOF packed bed. The unit layer contains MOF particles and air gap between particles. Particles are in contact with other particles in and outside this layer. Top right shows a unit cell we defined with one MOF particle. (c) Schematic diagram of the thermal resistance in one unit layer.

Table 2
Measured parameters of MOF powder samples.

Samples	Thermal conductivity of MOF crystal (W/(m·K))	Inter-particle contact conductance (μW/K)	Porosity of the compacted powder
UiO-66	0.11	0.0117	0.73
UiO-67	0.19	0.09	0.54
Cu-BTC	0.39	0.82	0.53

parts: hot-wire measurement and fitting. The fitting further amplifies the error of hot-wire measurement. The accuracy can be further improved by reducing the thermal conductivity measurement error of compacted MOF powder. It should also be noted that, the concept of separating thermal conductivity of porous particles and contact resistance as we proposed in this study not only works for transient hot wire method but also for other steady-state and transient methods including 3ω, thermal reflectance and so on.

4. Conclusion

In summary, we proposed a general method to derive the thermal conductivity of tiny MOF crystals based on the measurement of compacted powders. Three different MOF powders (UiO-66, UiO-67 and Cu-BTC) were chosen due to their facile synthesis, high yield, and varying structure properties, which we believe can be used as representative samples. They were tested under varying water contents with a transient hot-wire measurement. The increased thermal conductivity at low water contents can be attributed to the increased thermal conductivity of MOF particles resulting from the adsorbed water molecules inside micropores of MOFs. During this process, the contact resistances between particles remain unchanged. Based on a proposed BEMA model, we derived the thermal conductivity of single MOF crystal and contact resistance of contacting MOF particles separately. The obtained thermal conductivities are reasonably consistent with previously reported experimental results, validating our strategy for deriving thermal conductivity of tiny MOF crystals. Compared with conventional methods for measuring the thermal conductivity of MOF crystals, our strategy can be applicable to a great number of MOF crystals that cannot grow to the sizes in millimeters due to its easy operation and low requirement for sample preparation.

Conflict of interest

The authors declared that there is no conflict of interest.

Acknowledgement

This work was funded by the National Natural Science Foundation of China (51606082, 51606081) and the double first-class research funding with independent intellectual property of Institute of clean and renewable energy (ICARE) under the grant No of ICARE-RP-2018-HYDRO-001. We thank Lurong Ge and Chenyi

Wang for the contribution of hot-wire thermal conductivity measurements and Wei Li for the help in the schematic figures. We also thank the support from Analytical & Testing Center of Huazhong University of Science and Technology, China.

Appendix A. Supplementary data

Supplementary data to this article can be found online at https://doi.org/10.1016/j.ijheatmasstransfer.2019.04.018.

References

[1] H. Li, M. Eddaoudi, M. O'Keeffe, O.M. Yaghi, Design and synthesis of an exceptionally stable and highly porous metal-organic framework, Nature 402 (1999) 276.
[2] N.L. Rosi, J. Eckert, M. Eddaoudi, D.T. Vodak, J. Kim, M. Keeffe, O.M. Yaghi, Hydrogen storage in microporous metal-organic frameworks, Science 300 (2003) 1127–1129.
[3] H. Li, K. Wang, Y. Sun, C.T. Lollar, J. Li, H.-C. Zhou, Recent advances in gas storage and separation using metal–organic frameworks, Mater. Today 21 (2018) 108–121.
[4] J. Ren, B. North, Shaping porous materials for hydrogen storage applications: a review, J. Technol. Innov. Renew. Energy 3 (2014) 12–20.
[5] P. Camille, Present and future of MOF research in the field of adsorption and molecular separation, Curr. Opin. Chem. Eng. 20 (2018) 132–142.
[6] M. Zhang, Q. Dai, H. Zheng, M. Chen, L. Dai, Novel MOF-derived Co@N-C bifunctional catalysts for highly efficient Zn–Air batteries and water splitting, Adv. Mater. 30 (2018) 1705431.
[7] E.A. Dolgopolova, A.M. Rice, C.R. Martin, N.B. Shustova, Photochemistry and photophysics of MOFs: steps towards MOF-based sensing enhancements, Chem. Soc. Rev. 47 (2018) 4710–4728.
[8] M.J. Kalmutzki, C.S. Diercks, O.M. Yaghi, Metal–organic frameworks for water harvesting from air, Adv. Mater. 30 (2018) 170430.
[9] H. Kim, S. Yang, S.R. Rao, S. Narayanan, E.A. Kapustin, H. Furukawa, A.S. Umans, O.M. Yaghi, E.N. Wang, Water harvesting from air with metal-organic frameworks powered by natural sunlight, Science 356 (2017) 430–434.
[10] J. Purewal, D. Liu, A. Sudik, M. Veenstra, J. Yang, S. Maurer, U. Müller, D.J. Siegel, Improved hydrogen storage and thermal conductivity in high-density MOF-5 composites, J. Phys. Chem. C. 116 (2012) 20199–20212.
[11] Y. Ming, J. Purewal, D. Liu, A. Sudik, C. Xu, J. Yang, M. Veenstra, K. Rhodes, R. Soltis, J. Warner, M. Gaab, U. Müller, D.J. Siegel, Thermophysical properties of MOF-5 powders, Microporous Mesoporous Mater. 185 (2014) 235–244.
[12] D. Liu, J.J. Purewal, J. Yang, A. Sudik, S. Maurer, U. Mueller, J. Ni, D.J. Siegel, MOF-5 composites exhibiting improved thermal conductivity, Int. J. Hydrogen Energy 37 (2012) 6109–6117.
[13] T.A. Semelsberger, M. Veenstra, C. Dixon, Room temperature thermal conductivity measurements of neat MOF-5 compacts with high pressure hydrogen and helium, Int. J. Hydrogen Energy 41 (2016) 4690–4702.
[14] Z.-G. Qu, H. Wang, W. Zhang, Highly efficient adsorbent design using a Cu-BTC/CuO/carbon fiber paper composite for high CH_4/N_2 selectivity, RSC Adv. 7 (2017) 14206–14218.
[15] J.J. Purewal, D. Liu, J. Yang, A. Sudik, D.J. Siegel, S. Maurer, U. Müller, Increased volumetric hydrogen uptake of MOF-5 by powder densification, Int. J. Hydrogen Energy 37 (2012) 2723–2727.
[16] Y. Ming, H. Chi, R. Blaser, C. Xu, J. Yang, M. Veenstra, M. Gaab, U. Müller, C. Uher, D.J. Siegel, Anisotropic thermal transport in MOF-5 composites, Int. J. Heat Mass Transf. 82 (2015) 250–258.
[17] R.S. Prasher, X.J. Hu, Y. Chalopin, N. Mingo, K. Lofgreen, S. Volz, F. Cleri, P. Keblinski, Turning carbon nanotubes from exceptional heat conductors into insulators, Phys. Rev. Lett. 102 (2009) 105901.
[18] B. Cui, C.O. Audu, Y. Liao, S.T. Nguyen, O.K. Farha, J.T. Hupp, M. Grayson, Thermal conductivity of ZIF-8 thin-film under ambient gas pressure, ACS Appl. Mater. Interfaces 9 (2017) 28139–28143.
[19] W.D.C.B. Gunatilleke, K. Wei, Z. Niu, L. Wojtas, G. Nolas, S. Ma, Thermal conductivity of a perovskite-type metal-organic framework crystal, Dalt. Trans. 46 (2017) 13342–13344.
[20] B.L. Huang, Z. Ni, A. Millward, A.J.H. McGaughey, C. Uher, M. Kaviany, O. Yaghi, Thermal conductivity of a metal-organic framework (MOF- 5): Part II. Measurement, Int. J. Heat Mass Transf. 50 (2007) 405–411.
[21] B.L. Huang, A.J.H. McGaughey, M. Kaviany, Thermal conductivity of metal-organic framework 5 (MOF- 5): Part I. Molecular dynamics simulations, Int. J. Heat Mass Transf. 50 (2007) 393–404.
[22] X. Zhang, J. Jiang, Thermal conductivity of zeolitic imidazolate framework-8: a molecular simulation study, J. Phys. Chem. C. 117 (2013) 18441–18447.
[23] A. Schaate, P. Roy, A. Godt, J. Lippke, F. Waltz, M. Wiebcke, P. Behrens, Modulated synthesis of Zr-based metal–organic frameworks: from nano to single crystals, Chem. – A Eur. J. 17 (2011) 6643–6651.
[24] S. Øienødegaard, B. Bouchevreau, K. Hylland, L. Wu, R. Blom, C. Grande, U. Olsbye, M. Tilset, K.P. Lillerud, UiO-67-type metal–organic frameworks with enhanced water stability and methane adsorption capacity, Inorg. Chem. 55 (2016) 1986–1991.
[25] Q.M. Wang, D. Shen, M. Bülow, M.L. Lau, S. Deng, F.R. Fitch, N.O. Lemcoff, J. Semanscin, Metallo-organic molecular sieve for gas separation and purification, Microporous Mesoporous Mater. 55 (2002) 217–230.
[26] C.L. McCallum, T.J. Bandosz, S.C. McGrother, E.A. Müller, K.E. Gubbins, A molecular model for adsorption of water on activated carbon: comparison of simulation and experiment, Langmuir 15 (1999) 533–544.
[27] H. Furukawa, F. Gándara, Y.-B. Zhang, J. Jiang, W.L. Queen, M.R. Hudson, O.M. Yaghi, Water adsorption in porous metal–organic frameworks and related materials, J. Am. Chem. Soc. 136 (2014) 4369–4381.
[28] H.T. Aichlmayr, F.A. Kulacki, The effective thermal conductivity of saturated porous media, Adv. Heat Transf. 39 (2006) 377–460.
[29] A.D. Brailsford, K.G. Major, The thermal conductivity of aggregates of several phases, including porous materials, Br. J. Appl. Phys. 15 (1964) 313.
[30] A.M. Thiele, A. Kumar, G. Sant, L. Pilon, Effective thermal conductivity of three-component composites containing spherical capsules, Int. J. Heat Mass Transf. 73 (2014) 177–185.
[31] S.C. Cheng, R.I. Vachon, The prediction of the thermal conductivity of two and three phase solid heterogeneous mixtures, Int. J. Heat Mass Transf. 12 (1969) 249–264.
[32] S.C. Cheng, R.I. Vachon, Thermal conductivity of packed beds and powder beds, Int. J. Heat Mass Transf. 12 (1969) 1201–1206.
[33] K. Ridgway, K.J. Tarbuck, Random packing of spheres, J. Soc. Mater. Sci. Jpn. 17 (1967) 454–458.
[34] C.T. Hsu, P. Cheng, K.W. Wong, Modified Zehner-Schlunder models for stagnant thermal conductivity of porous media, Int. J. Heat Mass Transf. 37 (1994) 2751–2759.
[35] P. Zehner, E.U. Schulunder, Thermal conductivity of granular materials at moderate temperature, Chemie Ingenieur Technik 42 (1970) 933–941.
[36] L. Han, M. Budge, P. Alex Greaney, Relationship between thermal conductivity and framework architecture in MOF-5, Comp. Mater. Sci. 94 (2014) 292–297.